JOURNAL OF GEOPHYSICAL RESEARCH, VOL. ???, XXXX, DOI:10.1029/,

Observations of the relationship between ionospheric central polar cap and dayside throat convection velocities, and solar wind/IMF driving

W. A. Bristow,[1] E. Amata,[2] J. Spaleta[1], M. F. Marcucci[2]

Corresponding author: W. A. Bristow Geophysical Institue of the University of Alaska Fairbanks 903 Koyukuk Dr, Fairbanks AK 99775, USA, Bill.Bristow@gi.alaska.edu

[1]Geophysical Institute, University of Alaska Fairbanks, Fairbanks, Alaska, USA

[2]Istituto di Astrofisica e Planetologia Spaziali dell'NAF, Roma, Italia

Abstract.

Convection observations from the southern hemisphere SuperDARN network are presented and examined for their relationship to solar wind and interplanetary magnetic field (IMF) conditions, restricted to periods of steady IMF. Analysis is concentrated on two specific regions, the central polar cap and the dayside throat region. An example time series is discussed in detail with specific examples of apparent direct control of the convection velocity by the solar wind driver. Closer examination however shows that there is variability in the flows that can not be explained by the driving. Scatter plots and histograms of observations from all periods in the year 2013 that met the selection criteria are given and their dependence on solar wind driving is examined. It is found that on average the flow velocity depends on the square root of the rate of flux entry to the polar cap. It is also found that there is a large level of variability that is not strongly related to the solar wind driving.

1. Introduction

The Super Dual Auroral Radar Network (SuperDARN) observes plasma convection in the ionosphere in both the northern and southern hemispheres. In the southern hemisphere, the radar located at McMurdo Station, Antarctica, observes directly over the magnetic pole, which lies at a distance of about 1000 km from the radar; an optimal range for HF radar observations of convection [*Bristow et al.*, 2011]. A new pair of radars was added to the southern SuperDARN network in the Antarctic summer of 2012/2013 with radars at the US base South Pole Station, and the French-Italian base at Dome Concordia (Dome-C). This new pair of radars observes the region just equatorward of McMurdo station. Figure 1 shows the fields-of-view of the McMurdo, South Pole, and Dome-C radars. This observing geometry enables observations of the central polar cap plasma flow while simultaneously observing the auroral zone, which is ideal for studies of (for example) the day-side inflow region or the night-side outflow region. The dayside observations are particularly interesting since the cusp region is the main location where solar-wind energy is deposited in the Earth's magnetosphere, driving convection in the entire system. As Figure 1 shows, the South Pole and Dome-C fields-of-view cover the region just to the east of the 180° longitude line, which means that the dayside observations occur during the time interval between about 1700 UT and 2100 UT.

Development of plasma flow in the polar caps is a central topic of magnetospheric dynamics. Ever since *Dungey* [1961] described an open magnetosphere, we have had the concept of the solar wind electric field mapping along magnetic field lines into the polar cap. In that seminal paper, a twin-cell convection pattern was described resulting from this mapping along equipotentials from the solar wind into the ionosphere generating anti-sunward flow in the polar cap and sunward return flow within the region of closed magnetic field lines. The concept has developed over time into sophisticated models of the Earth's magnetosphere that include the distortion of the field by gas-dynamic forces and the expected modifications to the magnetic field configuration for different merging geometries [*Toffoletto and Hill*, 1989]. The concept of convection being driven by direct mapping of the solar wind electric field into the polar-cap ionosphere, however, leads to the unphysical conclusion that the flow velocity in a particular region of the ionosphere would correspond directly to the electric field of the specific region of the solar wind lying along the same magnetic field line. Such correspondence would at times lead to regions of compression and rarefaction of the ionospheric magnetic flux, which is not possible for physically realizable flow velocities. This understanding led *Siscoe and Huang* [1985] to describe patterns of convection in the ionosphere that differed from that due to direct mapping. The model for convection described in that paper and subsequent refinements [*Moses et al.*, 1987; *Moses et al.*, 1989; *Moses and Reiff*, 1991; *Lockwood et al.*, 1990; *Cowley and Lockwood*, 1992] has convection being the result of two somewhat independent reconnection processes. The first being dayside merging of the interplanetary magnetic field (IMF) with the Earth's magnetic field. The second being in the magnetotail, which closes flux previously opened by the dayside merging. In this scenario, the electric field along the dayside merging line maps into the ionosphere along the magnetic field and drives ionospheric convection. In magnetotail reconnection, it is not the solar wind electric field that drives convection (directly). Rather, it is the release of energy that has been accumulated in the lobes through convecting magnetic flux from the dayside.

Since the cusp driven ionospheric flow is excited by a mapping of the electric field in the reconnection region along the cusp magnetic field lines, the ionospheric speed should correlate best to metrics of the solar wind that attempt to characterize that process such as the Akasofu epsilon parameter [*Akasofu*, 1979] rather than the solar wind electric field itself.

In a recent paper *Newell et al.* [2007] examined the correlation between various measures of magnetospheric activity and a number of solar wind-magnetosphere coupling functions. They demonstrated that nearly every magnetospheric measure could be predicted with fairly high correlation by functions of solar wind parameters related to the dayside merging rate, with some of the correlations exceeding 0.8. While the paper did identify a "best" function, the differences in performance among the top few candidates were small. The main conclusion from that study was that the dayside merging rate was "the single largest correlate for most magnetospheric activity". In the work presented here, the Newell et al. *best* function was adopted for characterizing solar wind driving and is referred to as E_{MP} to signify the merging electric field at the magnetopause.

While there may be strong correlation between global measures of activity and solar wind driving parameters, the variability in those measures for a given driving level is large [*e.g. Bristow et al.*, 2004; *Lockwood et al.*, 2009]. To some extent the variability can be explained by accounting for the history of the magnetospheric state prior to an interval. *Lockwood et al.* [2009] examined the cross-polar-cap-potential, Φ_{PC}, as a function of the driving but separated intervals based on substorm phase. Figure 7 of that paper showed a significantly reduced level of variability in Φ_{PC} during intervals classified as "Quiet &

Growth" versus the variability in intervals described as "Disturbed AL". Even in the quiet intervals however, the spread in values about the trend lines was still large.

Simultaneous observations of flows localized in the cusp and central polar cap provide additional information on the degree to which dayside reconnection exerts control over convection in the system. It might be expected that since the dayside merging drives convection in the cusp region, flow in that region would correspond more closely to the solar wind driving than would flow in other regions. The expectation is that dayside reconnection excites high-speed flow in the cusp region that influences the flows at all latitudes and local times. However, the magnitude of influence should decrease with distance from the cusp but the correlation should remain high. The cusp flows appear in the *dayside throat* region, which is an identifiable feature of the convection patterns measured in the ionosphere.

In this study, observations from the full southern hemisphere SuperDARN network obtained during selected periods of the first year of operation of the South Pole and Dome-C radars, calendar year 2013, were used to form convection patterns using the standard SuperDARN potential mapping algorithm [*Ruohoniemi and Baker*, 1998]. The magnitude of these vectors was averaged within areas identified as the dayside throat and the central polar cap for each two minute period, producing time series of average convection in the two regions. In addition to producing time series, the data were accumulated in scatter plots and histograms and examined for various dependencies on IMF, solar wind, and each other.

Periods included in the study were chosen based upon the ACE IMF observations. Data were included from intervals in which the observed IMF components had only small fluctuations ($\sigma_B < 1$ nT) for periods of at least an hour. Choosing such intervals has two results. First, it helps to overcome the uncertainty in the propagation delay from the observing satellite to the point at which the observed IMF becomes effective at driving flow in the ionosphere. Second, it allows examination of flow evolution under steady driving, which may differ from flows under variable driving [*Lockwood et al.*, 2009].

2. Data presentation

Figure 2 shows the line-of-sight (LOS) velocity observations from McMurdo and the IMF observations from the ACE spacecraft during one of the intervals selected for study. The satellite observations were delayed by an amount calculated using an algorithm similar to that used to create the OMNI database [*e.g. Weimer and King*, 2008]. The algorithm estimates the position where a flux tube intersected the earth-sun line and uses the observed solar wind velocity to propagate from that point to the magnetopause. The figure shows ten hours of observations from 1200 UT (0455 MLT) to 2200 UT (1435 MLT) including the interval from about 1535 UT to about 2041 UT, which met the criteria for this study. The ACE observations show relatively steady southward IMF during most of the interval. Prior to 1535 UT the y-component varied between about -5 nT and +5 nT, and there was a positive excursion of the z-component between about 1500 and 1530, which was more variation than was acceptable. If the central cap velocity is determined solely by the IMF, based upon these observations the expected flow would be primarily antisunward with a fairly steady velocity for most of the period. In the interval, the McMurdo position rotated from near dawn through magnetic local noon, which occurs around 1930 UT. The look direction of the radar beam plotted in the figure rotates from perpendicular to the earth-sun line to parallel to it. If the central cap velocity were steadily antisunward, the observed LOS velocity would show a cosine dependence starting with zero velocity around 1330 UT, peaking around 1930 UT and dropping off after that time. The B_y component observed during the interval would modify this expectation somewhat, with the negative B_y observed in the early part of the interval adding a dawn-to-dusk velocity componenent, and the positive B_y observed in the latter portion yielding a dusk-to-dawn component. The actual pattern observed by McMurdo was similar to the expected, with a value near 0 at the beginning, increasing through the first half of the period, then decreasing toward the end. The observations through the interval show moderately variable flows of 0 m/s to about -900 m/s, where negative indicates velocity away from the radar. The peak observed value occurred just prior to 1800, which was about and hour and a half before the expected time of the peak at magnetic noon. For a 30 minute interval before about 1530 the line-of-sight velocity decreased and even briefly reversed from negative to positive.

A few features of the interval are typical of McMurdo observations. First, at times there is a clear response in the flows that can be associated with a specific observation in the IMF. For example, the IMF fluctuation observed around 1500 to 1530 UT clearly relates to the decreased LOS velocity observed in that time period. The brief sign change of the LOS velocity even appears to reflect the bi-polar fluctuation in the IMF B_y and B_Z components observed at the time. It should be noted that the decrease in LOS velocity begins some 20 minutes or so after the change in the IMF begins, however the brief sign change of the LOS velocity is simultaneous with the brief bi-polar IMF fluctuation. This discrepancy illustrates that while the delay between the IMF observation and the time at which it reached the magnetopause was estimated algorithmically accounting for tilts of the IMF planes, there is still uncertainty both in that delay, and in the time at which the IMF becomes effective in influencing convection after reaching the magnetopause. This should be kept in mind in when evaluating some of the later results presented in this manuscript. A second typical feature of the McMurdo observations is illustrated in the interval from about 1600 UT to about 2000 UT. The scatter in this interval was not continuous over area, rather it was characterized by distinct regions of irregularities receding from the radar. These regions are the signature that would be expected from polar-cap patches propagating across the central polar cap. Further, while the radar backscatter appears patchy, the magnitude of the velocity within the patches and over time remains relatively steady, corresponding to the roughly steady value of the IMF.

Convection patterns were formed for this interval using all available southern hemisphere SuperDARN observations. The patterns were generated using the potential mapping technique of *Ruohoniemi and Baker* [1998], which estimates global maps of the electrostatic potential that minimize inconsistency with the available observations. The technique expresses the potential as a summation of spherical harmonic functions with coefficients determined by a fit constrained by observed LOS velocities. In regions where there are no observations, the fit is constrained by a sampling from model convection patterns keyed to the IMF. Figure 3 shows the pattern for one two-minute interval with the fields of view of the McMurdo, South Pole, and Dome-C radars highlighted. The figure displays the region between -55° and the south magnetic pole, with noon at the top, midnight at the bottom, and dawn and dusk on the left and right respectively. The small clock-dial in the upper right corner shows the observed IMF $B_y - B_z$ components that were observed at ACE at the calculated delay time, about 70 minutes prior to the interval. The convection arrows shown on the figure illustrate the areas where there were observations from at least one radar during the interval. The vectors were determined from the fitted convection pattern rather than directly from the measurements. This method tends to smooth the results but ensures that the vectors are divergence free. It likely reduces the peak velocity values from those truly present. The figure shows good data coverage of both the dayside throat and the central cap, which persisted throughout the period of interest. The red circle of 5° radius centered on the magnetic pole represents the area over which vectors were averaged to get the central-polar cap velocity. The box centered at 75.5° magnetic latitude and 1100 magnetic local time (MLT) represents the approximate averaging area identified as the throat. The location of the box was determined by inspecting the maps for each two-minute period in the interval. While there was evolution of the pattern over time and some motion of the throat, the 3° latitude width and 1-hour MLT width of the averaging area captured the motion. The convection pattern was somewhat complex but was two-celled as would be expected from the IMF. The estimated cross-cap potential was about 50 kV. The observed flows show antisunward convection in the central cap with a speed of around 500 m/s. The day side throat velocity was somewhat higher speed and was directed into the cap but across noon from dawn to dusk. Flow observed near 0300 MLT and 0600 MLT show the return flow was for the most part contained above 65°.

Figure 4 shows the time series of spatially averaged velocity magnitude for the two regions, with the blue line indicating a calculation of the solar wind driving, $E_{MP} = v_x^{4/3} B_t^{2/3} \sin^{8/3}(\theta/2)$, where B_t is the magnitude of the component of the IMF transverse to the magnetopause, and θ is the IMF clock angle ($\theta = \arctan(B_y/B_z)$). The units of this function are discussed in *Cai and Clauer* [2013], where the authors empirically determined that a normalization factor of 100 makes the unit Wb/s. As discussed in the introduciton, this product characterizes the dayside merging rate and has been shown to correlate well with measures of magnetospheric activity [*Newell et al.*, 2007]. The black lines indicate the dayside throat flow speed and the red lines indicate the central polar cap flow speed. The dashed lines show 16-minute averages of the 2-minute values, which are shown by the solid lines. The dotted lines adjacent to the solid lines show the statistical uncertainty. E_{MP} remained steady up until about 1930 UT when it began a gradual decrease until the end of the interval. While the driver remained relatively steady or was slowly decreasing, the flow velocities in both regions showed substantial variations during the interval. The dayside flow ranged between 500 m/s and 1700 m/s, and exceeded 1500 m/s for an extended time. Additionally, the dayside flow showed higher variability in both short term excursions of a few minutes and in the longer term averages shown by the dashed lines. At times the short term excursions exceeded 500 m/s amplitude above or below the average over tens of minutes. The longer term average value increased from 500 m/s to 1700 m/s over the time from the beginning of the interval and 1800 UT, then decreased from 1800 UT to 1910 UT to about 1000 m/s and rose again over the remaining time in the interval. The central cap average value ranged between about 350 m/s and 700 m/s; exceeding 700 m/s only briefly at around 1740 UT. It shows a gradual increase from the beginning of the period up until about 1740 UT, followed by a gradual decrease until the end of the period. There was short term variability in the central cap flow, but it was a substantially lower amplitude than that in the dayside flow. Some of the fluctuations observed in the central cap appear to correlate to the dayside fluctuations, but the correlation coefficient calculated for the overall interval was only 0.475. The correlation coefficient peaked for a zero time lag between the two time series.

The central cap flow, while less variable than the dayside flow, still varied by over a factor of two. The dayside flows varied by more than a factor of three. Such variations without an obvious solar wind driver are likely related to internal magnetospheric processes. The concepts of the expanding-contracting polar cap model for convection [*Milan et al.*, 2007] could potentially explain the some of the observations, though only partially. Examination of magnetometer observations from the IMAGE chain in northern Europe (http://space.fmi.fi/image/index.html) during the interval indicate that there was substorm activity. It appears that there was a growth phase that started around 1500 UT or earlier, followed by an expansion phase onset around 1700 UT, and a recovery phase that began around 1715 UT and lasted until at least 1900 UT. The timing of these magnetometer signatures don't directly align with the changes in the observed flow velocities, however arguments could be made to associate them. For example, the increase in the dayside throat flow velocity could be understood from the increasing polar cap diameter during period prior to expansion onset. If the low-latitude convection boundary did not move equatorward at the same rate as the polar cap boundary, the flow would have become constricted and if the reconnection rate remained unchanged, the velocity would have had to increase to supply the same amount of flux. At some point after expansion onset, reconnection in the tail would begin to close open flux and the polar cap diameter would begin to decrease, which would eventually decrease the constriction of the dayside convection. In addition to the increase due to geometrical changes, the doubling of the polar cap velocity over the period up until about 1730 UT could have been due to the potential associated with magnetotail substorm processes. It should be noted, however, that the influence of the night-side reconnection processes is expected to decrease with distance, so should be reflected more strongly in the central cap flow than in the dayside flows [*Cowley and Lockwood*, 1992].

To further investigate the relationship between solar wind forcing and convection speeds, a large database of similar intervals was examined. The level-2 ACE magnetic field data from 2013 were searched for periods in excess of an hour within which the standard deviations of the y- and z-components did not exceed 1 nT. Figure 5 shows the resulting occurrence histograms of one-minute intervals for each component of the IMF and their absolute deviations. The deviations were calculated for each interval by subtracting the average value for the period from the observed value at each instant. The histograms show that the x-,and y-components were fairly uniformly distributed between +5 nT and -5 nT, while the z-components appear normally distributed and concentrated around 0 nT, but with significant density in the distribution out to about $\pm$ 5 nT. The deviations for all three components were small. The plasma data observations from ACE were also examined for the intervals but are not shown in a figure. The average radial velocity was 415 km/s with a standard deviation of 80 km/s. The average number density was 3.5/cc with a standard deviation of 2.6/cc. The absolute deviations of both the velocity and density were small, the full width at half maximum of the velocity deviation distribution was about 20 km/s, while the density deviation full width was 0.5/cc. In all about 4504 hours of observations met the criteria.

Southern-hemisphere convection patterns were formed every two minutes of the steady-IMF intervals. For each pattern, the velocity magnitudes were spatially averaged in the throat and cap as described above. To determine the location of the throat, an average convection pattern was formed for the each steady IMF interval and the region between

75° and 80° magnetic latitude, and between 1000 MLT and 1400 MLT was searched to find the location with the maximum time average poleward velocity. That location was identified as the average throat for the entire steady-IMF interval and all points within the area ± 1.5°magnetic latitude and ±0.5 hours of MLT from that point were averaged to determine the throat velocity for each two-minute interval. The averages were included in this study only if a minimum of five vectors fell within the throat region and a minimum of ten vectors fell within the central-polar cap region. With these restrictions, 3443 hours met the criteria for the central polar cap, 538 hours met the criteria for the throat, and just 435 hours met the criteria for both the throat and the central cap simultaneously.

Figure 6 shows histograms of the observed velocity magnitudes for the whole database for both the central polar cap (a) and the throat (b). The two distributions show some similarities and some differences. Speeds in both regions are concentrated below about 1000 m/s, and show more velocities below the mean than above the mean. The central-cap distribution peaks at a velocity of around 200 m/s, an average velocity of 233 m/s, a standard deviation of 139 m/s, and shows very few velocities below 50 m/s. The throat distribution extends to higher velocities, with an average of 561 m/s and a standard deviation of 311 m/s. The smooth curves superposed on the histograms are Rayleigh distributions calculated using the means and deviations of the histograms and scaled by the peak number of observations. Both smooth curves appear to represent the respective distributions fairly well. In addition, it is interesting to note that the central-cap distribution shows no recorded velocities over 900 m/s. Examples of velocities in the central cap region of over 1000 m/s can be found in a broader database, however none were observed in the set used here. This may indicate a difference between steadily driven intervals and general intervals.

The observations for both regions were examined versus a number of parameters characterizing the solar wind and IMF driving of the magnetosphere. All of the comparisons gave similar results in the sense that higher driving led to higher average velocities but in each case there was a large spread about the average, with the standard deviations being about the same magnitude. Two sets of figures illustrating the different driving functions are presented here. First, Figure 7 shows a scatter plot of observed velocity magnitude versus the product of the solar wind velocity x-component, v_x, and the IMF z-component, B_z, which gives the y-component of the solar wind electric field. Each point in the scatter plot represents the average velocity observed in the central polar cap from a two-minute interval. The points are color coded by the IMF y-component. IMF B_y could influence the velocities in two ways. First, it could increase the dayside reconnection rate leading to higher observed velocities. Second, distortion of the convection pattern caused by a finite B_y could concentrate the flow into a channel and lead to either higher or lower velocities for the same applied potential depending on the location of the channel for a given value of B_y. The figure does not show any clear evidence of a B_y dependence. The green diamonds show the mean calculated for bins of 0.5 mV/m of solar wind electric field. Vertical bars are plotted at each diamond indicating the uncertainty in the means determined from the standard deviation divided by the square root of the number of observations. While the spread of the points is large, the number of points is also large, which yields a small uncertainty as is illustrated by the short length of the bars. The standard deviations ranged from 103 m/s up to about 140 m/s, while the number of points ranged from about 400 up to over 16,500, resulting in uncertainties ranging from less than a meter per second up to about 7 m/s. For positive values of v_xB_z (southward IMF), there is a clear trend of increasing cap velocity with increasing solar wind electric field. Between about -1 mV/m and 3 mV/m solar wind electric field, the increase is relatively linear with a value of about 80 (m/s)/(mV/m). Other than the point at $v_xB_z = 2.5mV/m$ lying below the trend line, there is no evidence for saturation of average cap velocity for higher driving in these data. For negative values of v_xB_z ¡ -2 mV/m (northward IMF) there is also a trend of increasing average velocity magnitude with increasing v_xB_z magnitude.

Figure 8 shows the same data plotted versus E_{MP}. The trend of the data shows a similar pattern to that illustrated in Figure 7. The average cap velocity increases with increasing E_{MP}, though there is a large spread of points around the average. In addition to the colored points corresponding to 2-minute intervals, there are black diamonds representing the average values over 15-minute intervals. The distribution of the 15-minute average points is essentially the same as the distribution of the 2-minute points. This lack of reduction in spread illustrates that during an individual interval of steady driving parameter the cap velocity does not show large point-to-point variability. Rather it shows secular increases and decreases of longer duration, as was seen in Figure 4. The spread of values indicates that the polar cap velocity during different intervals with similar solar wind conditions can have significantly different values. That is, similar driving can lead to very different responses. As in Figure 7, the green diamonds and connecting line represent the average values for the 10 bins of E_{MP}. In this figure the superposed blue line is a linear fit of the velocity vs the square root of E_{MP}. At E_{MP} values between about 5×10^5 Wb/s and 1×10^6 Wb/s, the diamonds could be fit equally well with either a linear dependence on E_{MP} itself or its square root. At low values however, below about 2×10^5 Wb/s, the rapid increase of average velocity with increasing E_{MP} is clearly better represented by the square root dependence than by a linear dependence.

To further examine the dependence of polar cap plasma velocity on solar wind driving, Figure 9 shows histograms of observed velocity for increasing values of E_{MP}. The panels are organized with the lowest range of E_{MP} in the lower left, increasing to the right and upward. On each histogram a skew-normal distribution is superposed scaled to match the total number of observations in the histogram. The average and standard deviation of the distribution are printed in the upper right corner of each frame. The average value is seen to increase systematically with increasing E_{MP} range, which simply illustrates the trend shown in the scatter plot. The standard deviation however, remains relatively constant from range to range, with the value between 107 m/s and 148 m/s for all frames. With the exception of the lowest frame and the highest four frames, the value was around 120 m/s. For the lowest values of driving, the histograms show significant skew toward low velocity.

Figure 10 and Figure 11 show the throat velocity observations in the same formats as those given for the cap velocity in Figures 8 and 9. As was illustrated in Figure 6, the range of velocities observed in the throat extends to higher values than those in the central cap, with significant numbers of observations up to 1500 m/s and beyond. There is a trend of velocity increase with increasing E_{MP} over the range where there were significant numbers of observations. As was the case with the central cap velocity observations, the trend is not linear and for low values of E_{MP} the slope is steeper than it is for values above about 2.5×10^5 Wb/s. The blue line superposed on the figure is a linear fit of the velocity vs the square root of E_{MP}. The histograms of throat velocity show similar behavior to those in the central cap, though also with higher parameter values. The average velocities for each bin are about twice those in the cap. The standard deviations also remain fairly constant from bin-to-bin, but have a range from about 250 m/s up to about 300 m/s.

As a final examination of the data, Figure 12 displays a scatter plot of observed central cap velocity vs the observed throat velocity when simultaneous determinations were available. As would be expected from the previous figures, the cap velocity increases with increasing throat velocity, but there is a broad spread about the trend. The trend appears to be linear with a slope of about 0.18 (m/s)/(m/s). At the lowest values of throat velocity, the average velocities is about the same in the two regions. At the highest values of throat velocity, the cap velocity is less than half the throat velocity. The standard deviation of the cap velocities about the trend line is fairly constant around 100-120 m/s over the full range of throat velocities. This is a lower deviation than the value obtained when binning the cap velocities versus the solar wind driving, but not significantly lower. This variability indicates that there are factors influencing the two regions that were not considered here. A time delay between the two regions in response to solar wind driving is one possibility. Another is the relative sizes of the polar cap and the throat region. A certain potential value applied across a narrow throat gives a higher velocity than the same potential applied across a broad throat. The convection velocity in a region depends on the length over which a potential is applied. A common driver acting simultaneously in both regions would lead to very different comparisons for the case of a narrow throat and broad polar cap versus a broad throat and small polar cap.

3. Discussion

The observations presented here examine the relationship between solar wind driving and the plasma flow velocities observed in the ionosphere, focusing on two specific regions: the dayside throat and the central polar cap. The goals of the study were to examine the characteristics of the flow, to examine their dependence on solar wind driving, and to examine the interrelationship between the flows in the two regions. While many studies have examined the relationship between solar wind quantities and global measures of the magnetospheric state [*e.g. Reiff et al.*, 1986; *Newell et al.*, 2007; *Bristow et al.*, 2004; *Lockwood et al.*, 2009; *Bristow and Spaleta*, 2013], there is value in looking at specific regions in the same context. There may be reasons why one would expect a more direct relationship between local quantities in these regions and the driving functions than might be expected for global quantities and the same functions. For example, if reconnection at the dayside magnetopause is the primary driver of convection, one might expect the relationship between the flow in the dayside throat and E_{MP} to be closer there than in other regions of the convection pattern. Likewise, if the mapping of the solar wind electric field along magnetic field lines were responsible for driving convection, the central cap flow should be closely related to that quantity. Further, in a space weather context, local quantities often are the thing of interest. For example, when estimating the probability of scintillation causing irregularities developing in a specific region, it is the plasma flow over that region that is important, rather than something like the value of the cross-cap potential.

As was illustrated in Figure 2, the flows often show a nearly direct relationship to solar wind driving. The IMF transition that occurred in the interval around 1500 UT to 1530

UT was coincident with the observed slowing of the flow. There is even a small bipolar signature where the LOS velocity changed sign for a few minutes that corresponded to a similar signature in the IMF B_z and B_y components. After that brief interval, the IMF returned to being steadily southward, and the flows returned to being fairly steady and higher speed. A similar IMF change occurred at the end of the interval, about 2030 UT, when the z-component turned positive and there was a coincident decrease in the observed LOS velocity.

While such coincidences in the observations indicate direct control, looking at the total time interval shows that there is more to the picture. Figure 4 shows that, while the central cap flows were less variable than the dayside throat flows, they still varied by a factor of two when the solar wind driving was essentially unchanged. The driving was equally steady whether it is calculated form E_{MP} or from the solar wind electric field. The variability can be explained at least in part by considering additional driving of convection coming from the observed substorm and the associated magnetotail reconnection.

Short term variability of magnetospheric activity driven by dayside merging would be expected if merging was not a continuous processes. The nature of dayside merging is a long-standing debate in the space physics community with evidence supporting both quasi-steady [*e.g. Newell and Meng*, 1995] and strongly-pulsed merging [*e.g. Lockwood*, 1996]. There was even one recent study in which two intervals of energetic ion observations from the Polar space craft were examined, with one showing clear evidence of pulsed merging while the other showed continuous merging [*Trattner et al.*, 2015]. There have been a number of ground-based studies presenting convection observations in the cusp region that were attributed to transient merging events [*e.g. Greenwald et al.*, 1999; *McWilliams et al.*, 2001]. In one case [*Greenwald et al.*, 1999] the transient was associated with a significant increase in the convection velocity just poleward of the cusp region with a time scale similar to the velocity fluctuations illustrated in Figure 4, while in another [*McWilliams et al.*, 2001] the convection velocity remained steady while the merging signature propagated through the region of observation. The short term fluctuations of velocity observed in this study could be interpreted as support for transient dayside merging, however no conclusions could be drawn without additional observations to indicate merging signatures in the regions of the fluctuations.

The direct dependence and variability are further illustrated by the scatter plots and histograms, which show that the average values of flow speed in both the throat and the central cap increase with increased driving, however the variability about the trends is large. In both regions, the change in the average value over the full range of driving examined was less than 2.5 times the standard deviation of the lowest bins. In the central cap the average value in the lowest bin was 207 m/s and the standard deviation was about 120 m/s, while in the highest bin the average value was 477 m/s. Hence, predicting a velocity based upon the IMF and solar wind observations would have large error bars. Predicting the velocity is of course exactly what one does when using an empirical convection model keyed to the IMF. The significant differences in convection response to solar wind driving has been noted by other authors [*e.g. Lockwood et al.*, 2009]

The appearance of the scatter plots in this paper is similar to equivalent plots of global parameters given in other papers. The plots show a significant density of points to about plus and minus half the low end average value. For example, plots of the polar cap potential have a low end average value around 40 kV with significant numbers of points at least ±20 kV about that value. Here, the low end average value in the central cap is 200 m/s, and the deviation is about 100 m/s. The spread of points may increase some at the higher driving levels, however it doesn't change by much. The deviations given in Figures 9 and 11 increase with increased driving, but the increase is small. In the central cap the average deviation is 126 m/s, with the value in the lowest bin being 107 m/s and the value in the highest bin being 145 m/s. This may be an indication that the processes creating the variability are not directly related to the solar wind driver.

While having the histograms of convection velocity is useful for understanding the dependence of the flows on the solar wind parameters, they also provide a way of estimating the probability of observing ranges of velocity for specified conditions, which is arguably the most appropriate way of using IMF and solar wind observations for predicting convection. For example in the lowest range of E_{MP} (lower left of Figure 9), the probability of observing a velocity greater than 500 m/s in the polar cap is low, just 1.4%, while in the throat region it was significantly higher, about 25%. In the highest range examined, the probability of observing a velocity greater than 500 m/s in the central cap is 43%, and about 78% in the throat. In both regions, the probability increases monotonically with increasing E_{MP}. It is also interesting to note that there is a finite probability of observing a low velocity for all values of E_{MP}. The probability of observing a speed of less than 200 m/s is about 50% in the lowest bin, decreasing monotonically with increasing E_{MP} to a value 2.5% in the highest bin.

Another feature of the observations is that the flow speed in both regions is greater than zero for all levels of driving. It should be noted that the SuperDARN radars are biased against measuring a zero convection velocity. The radars measure the Doppler shift of signals scattered form field-aligned plasma density irregularities, which are formed by instabilities in the ionosphere, usually assumed to be the gradient-drift instability. Gradient-drift irregularities form when there is a finite flow velocity across an existing density gradient. Hence, a non-zero flow velocity is required for the irregularities to form. In addition, the standard SuperDARN data processing algorithms for estimating the Doppler shift excludes scatter that can not be distinguished from ground scatter, which comes from signals scattered from the ground after reflection from the ionosphere. The criteria for designating a received signal as ground scatter are that the velocity is below 30 m/s and the spectral width is below 90 m/s. It is rare for signals in the throat and polar cap regions to be labeled as ground scatter since one or both of these criteria is nearly always exceeded. Further, for the southern central polar cap, ground-scatter would have to come from the 3000 m thick polar ice cap, which is not observed. Even with the inability to make zero-velocity observations, it is likely that the observed roll off of the histograms of observed velocity below 200 m/s is geophysical rather than an artifact of the observations or processing. The velocity bins used in Figure 9 were 20 m/s in width, so the lowest two bins could potentially be influenced by the ground-scatter criterion. Even in the lower left hand frame, the lowest solar wind driving, the distributions show a steep roll off beginning at a 100 m/s or above. There is not an abrupt decrease in counts in the two lowest velocity bins, rather the counts appear to follow continuously from the curve through higher velocity bins. The binning in Figure 11 is coarser, however the roll off at low velocities is similar to that in the central cap. From this it can be concluded that under nearly all circumstances there is a finite convection velocity.

The plasma velocity's apparent square root dependence on E_{MP} may provide further support to reconnection driving convection rather than direct mapping of the solar wind electric field. E_{MP} characterizes the rate at which magnetic flux enters the polar cap. If the average area of the polar cap increases linearly with E_{MP}, then the average diameter increases as the square root of E_{MP}, which would translate to the average convection velocity having the same dependence.

4. Summary and Conclusions

One of the purposes of this study was to examine solar wind and IMF control of convection velocity in the central polar cap and in the dayside throat region. The observations showed good correspondence between flows and the solar wind, illustrating both direct correlation between specific IMF signatures and signatures in the flows, and in the increased average flow velocity with increased solar wind driving. There was, however, significant variability in the flow that was not observed in the driver. Some of that variability could be attributed to substorm activity, though probably not all. The short-term variations of as much as 500 m/s observed in the dayside flows occurred over much shorter time scale than the substorm time scale, and they occurred throughout the interval, not just in a certain substorm phase.

The characteristics of the flow in the two regions were similar in distribution but with higher average value and higher deviation in the throat than in the cap. The average values and the deviations were both about a factor of two larger in the throat. Flows in both regions showed a similar dependence on E_{MP} and in the average were fit well by the velocity being proportional to the $\sqrt{E_{MP}}$. The shapes of the distributions were also similar and were well represented by skew-normal distributions, with the amount of skew decreasing for higher driving levels.

The stated expectation given in the introduction was that the influence of dayside merging at the magnetopause would be strongest in the dayside flows and would decrease with distance. It is certainly true that the flow speed was higher in the throat than in the central cap, but that is likely the result of a geometrical effect since the flow is concentrated in a narrower region. If anything, the dayside flows showed more variability than the central cap flows with large amplitude fluctuations, occurring on time scales of tens of minutes, that were not observed in either the driver or in the central cap flow.

The primary conclusion that can be drawn from this set of observations is that the flow velocity in specific regions appears to be predictable with about the same level of precision as global-scale measures of magnetospheric activity. With this level of precision, the best use of solar wind observations in a predictive sense is to forecast probabilities for parameter values rather than predicting the specific values. While such forecasts may not be of use in the current generation of ionospheric specification models, a new generation of empirical convection models could be produced that would generate a time variable convection pattern with the same statistics as the observations.

Acknowledgments. The research reported here, including the operation of the McMurdo and South Pole SuperDARN radars, was supported by NSF grant PLR09044270 from the Division of Polar Programs. The installation and operation of the Dome-C radar is supported by the Programma Nazionale di Ricerche in Antartide (PNRA Italy) and the Institut Polaire Francais (IPEV France). The SuperDARN network is supported by equivalent governmental science agencies in the partner nations. All SuperDARN obser-

vations used in this study are available from the SuperDARN database. The IMF and solar wind observations were obtained from the NASA Space Physics Data Facility web page.

References

Akasofu, S.-I. (1979), Interplanetary energy flux associated with magnetospheric substorms, *Planet. Space Sci.*,*27*,425-431, doi:10.1016/0032-0633(79)90119-3

Bristow, W. A., R. A. Greenwald, S. G. Shepherd, and J. M. Hughes (2004), On the observed variability of the cross-polarcap potential, J. Geophys. Res., 109, A02203, doi:10.1029/2003JA010206.

Bristow, W. A., J. Spaleta, R. T. Parris (2011), First observatoins of ionospheric irregularities and flows over the south geomagnetic pole from the SuperDARN HF radar at McMurdo Station, Antarctica, *J. Geophys. Res.*,116,A12325, doi: 10.1029/2011JA016834RR

Bristow, W. A., J. Spaleta (2013), An investigation of the characteristics of the convection-reversal boundary under southward interplanetary magnetic field. J. Geophys. Res., DOI: 10.1002/jgra.50526

Baker, K. B., J. R. Dudney, R. A. Greenwald, M. Pinnock, P. T. Newell, A. S. Rodger, N. Mattin, and C.-I. Meng (1995), HF radar signatures of the cusp and low-latitude boundary layer, *J. Geophys. Res.*, 100(A5), 7671-7695

Cai, X., and C. R. Clauer (2013), Magnetospheric sawtooth events during the solar cycle 23, J. Geophys. Res. Space Physics, 118, 6378-6388, doi:10.1002/2013JA018819.

Cowley, S. W. H., and M. Lockwood (1992), Excitation and decay of solar wind-driven flows inthe magnetosphere-ionosphere system. *Ann. Geophys.*, 10, 103-115

Dungey, J. W. (1961), Interplanetary magnetic field and the auroral zones, *Phys. Rev. Lett.*,6,47

Greenwald, R. A., J. M. Ruohoniemi, K. B. Baker, W. A. Bristow, G. J. Sofko, J. - P. Villain, M. Lester, and J. Slavin (1999), Convective response to a transient increase in dayside reconnection, *J. Geophys. Res.*, 104(A5), 10007-10015, doi:10.1029/98JA02723.

Lockwood, M., S. W. H. Cowley, and M. P. Freeman (1990), The excitation of plasma convection in the high-latitude ionosphere., *J. Geophys. Res.*, *95*, A6, 7961-7972

Lockwood, M., (1996) The case for transient magnetopause reconnection. *EOS*, 77, 26, 1996

Lockwood, M., M. Hairston, I. Finch, A. Rouillard (2009)Transpolar voltage and polar cap flux during the substorm cycle and steady convection events *J. Geophys. Res.*, *114*, A01210, doi:10.1029/2008JA013697

McWilliams, K. A., T. K. Yeoman, S. W. H. Cowley (2001), Two-dimensional electric field measurements in the ionospheric footprint of a flux transfer event. *Ann. Geophys.*, 18, 1584-1598

Milan, S. E., G. Provan, B. Hubert (2007), Magnetic flux transport in the Dungey cycle: A survey of dayside and nightside reconnection rates, *J. Geophys. Res.*, *112*, A01209, doi:10.1029/2006JA011642

Moses, J. J., G. L. Siscoe, N. U. Crooker, D. J. Gorney (1987), IMF B_y and day-night conductivity effects in the expanding polar cap convection model. *J. Geophys. Res.*,*92*, A2, 1193-1198

Moses, J. J., G. L. Siscoe, R. A. Heelis, J. D. Winningham (1989), Polar cap deflation during magnetospheric substorms. *J. Geophys. Res.*,*94*, A4, 3785-3789

Moses, J. J. and P. H. Reiff (1981) Polar Cap Convection: Steady State and Dynamic Effects, in Magnetospheric Substorms (eds J. R. Kan, T. A. Potemra, S. Kokubun and T. Iijima), American Geophysical Union, Washington, D. C.. doi: 10.1029/GM064p0375

Newell, P. T., C.-I. Meng, (1995) Cusp low-energy cutoffs: A survey and implications for merging, *J. Geophys Res.*, 100, A11, 21,943-21,951.

Newell, P. T., T. Sotirelis, K. Liou, C.-I. Meng, and F. J. Rich (2007), A nearly universal solar wind-magnetosphere coupling function inferred from 10 magnetospheric state variables, *J. Geophys. Res.*, 112, A01206, doi:10.1029/2006JA012015.

Reiff, P. H., R. W. Spiro, T. W. Hill, Dependence of polar cap potential drop on interplanetary parameters., *J. Geophys. Res.*,*86*, A9, 7639-7648

Reiff, P. H., and J. G. Luhmann (1986), Solar wind control of the polar-cap voltage, in Solar Wind-Magnetosphere Coupling, edited by Y. Kamide and J. A. Slavin, pp. 453 476, Kluwer Acad., Norwell, Mass.

Ruohoniemi, J. M., K. B. Baker (1998), Large-scale imaging of high-latitude convection with Super Dual Auroral Radar Network HF radar observations, *J. Geophys. Res.*, *103*, 20,797

Siscoe, G. L., T. S. Huang (1985), Polar cap inflation and deflation, *J. Geophys. Res.*, *90*, A1, 543-547

Toffoletto, F. R., and T. W. Hill (1989), Mapping of the solar wind electric field to the Earth's polar caps, *J. Geophys. Res.*, 94, A1, 329-347.

Trattner, K. J., T. G. Onsager, S. M. Petrinec, and S. A. Fuselier (2015), Distinguishing between pulsed and continuous reconnection at the dayside magnetopause, *J. Geophys. Res. Space Physics*, 120, doi:10.1002/2014JA020713.

Weimer, D. R. and J. H. King (2008), Improved calculations of interplanetary magnetic field phase front angles and propagation time delays, *J. Geophys. Res.*, *113*, A01105, doi:10.1029/2007JA012452.

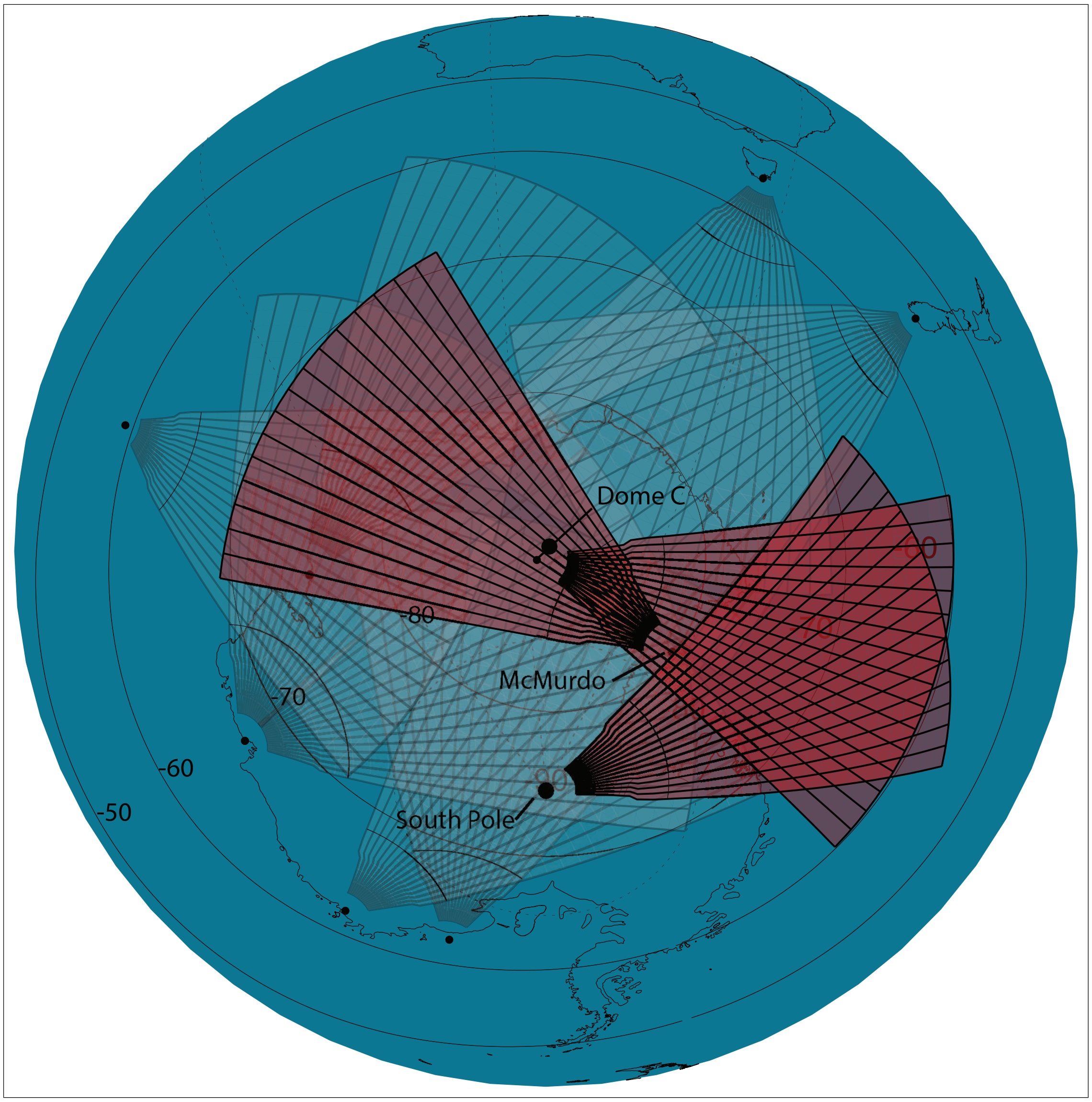

Figure 1. Fields-of-view of the McMurdo, South Pole, and Dome-C radars over contours of magnetic latitude. The radars are located at the vretices of the wedges. The radars sample the returns from the red shaded areas, which extend to 3500 km range from the radar sites. The rest of the southern hemisphere SuperDARN radar fields of view are shaded light gray.

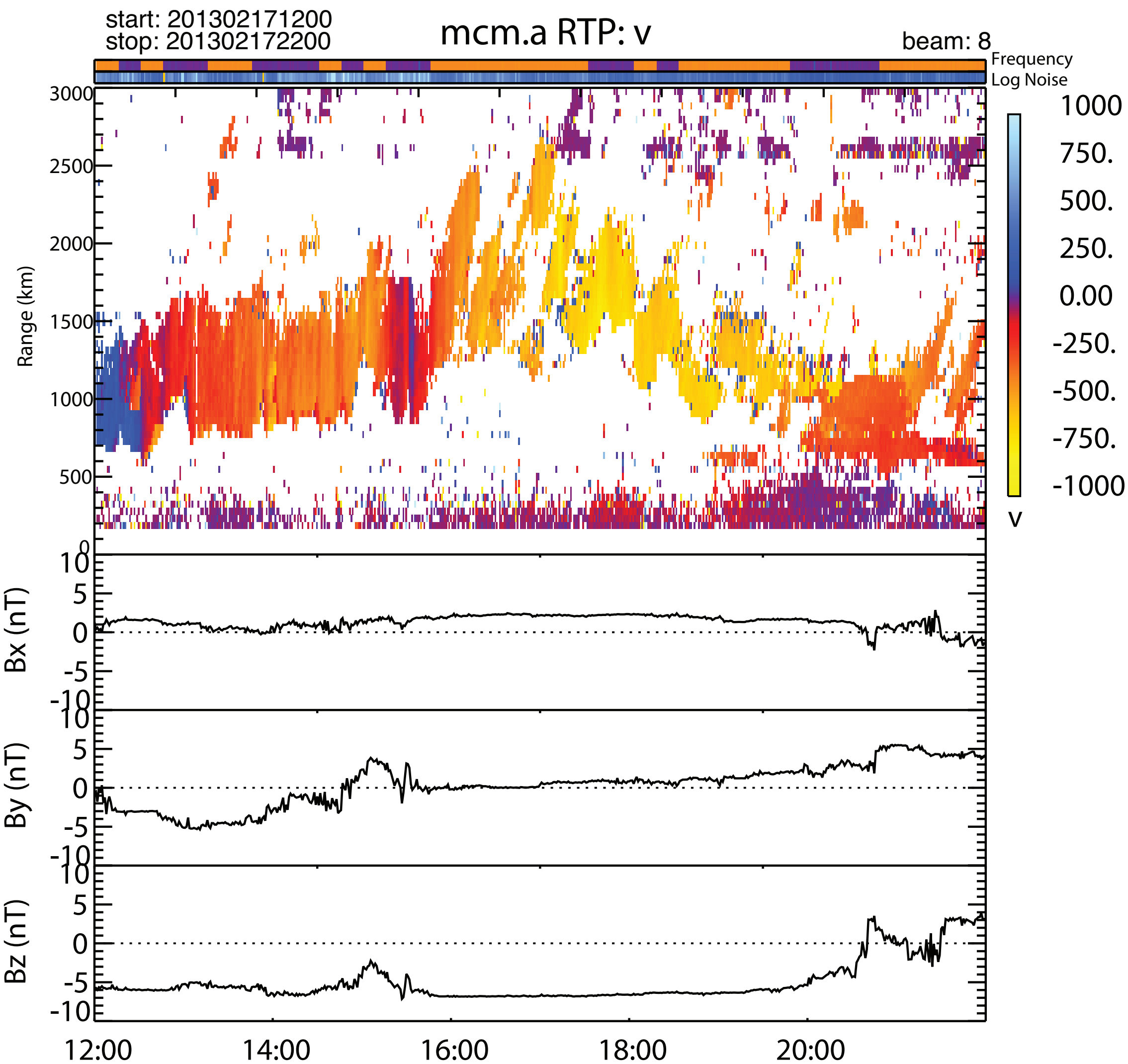

Figure 2. Range-time-velocity plot for returns observed by the McMurdo radar along its central beam, and IMF observations from the ACE space form February 17, 2013 between 1200 UT and 2200 UT. Figure shows the three components B_x, B_y, and B_z in GSM coordinates. The IMF values have been time delayed to the assumed position of the magnetopause

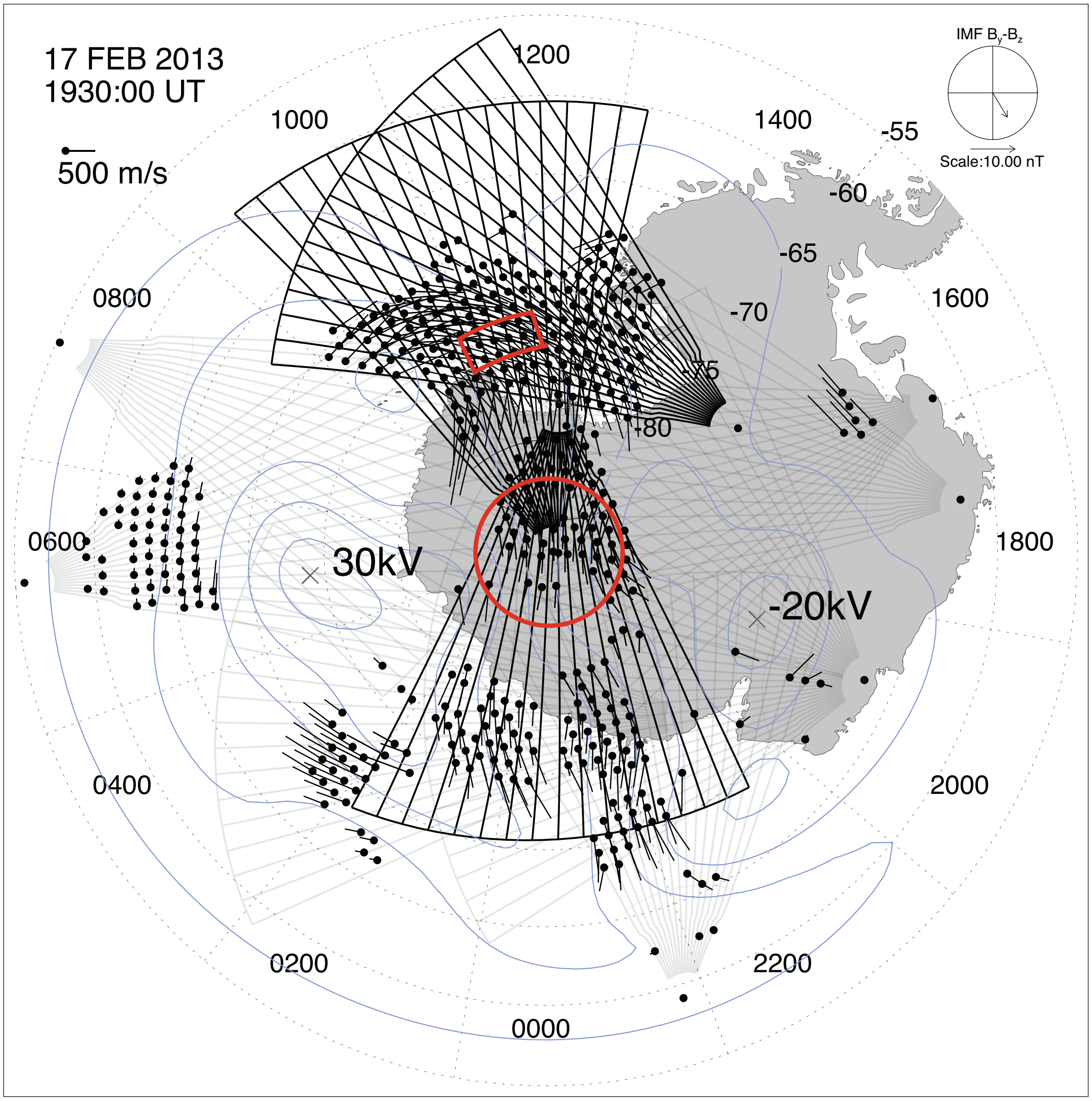

Figure 3. Convection map for 1930 UT on February 17, 2013. Fields of view of the McMurdo, South Pole, and Dome C radars are superposed. The red circle at 85° indicates the area defined as the central polar cap. The red box indicates the area defined as the dayside throat.

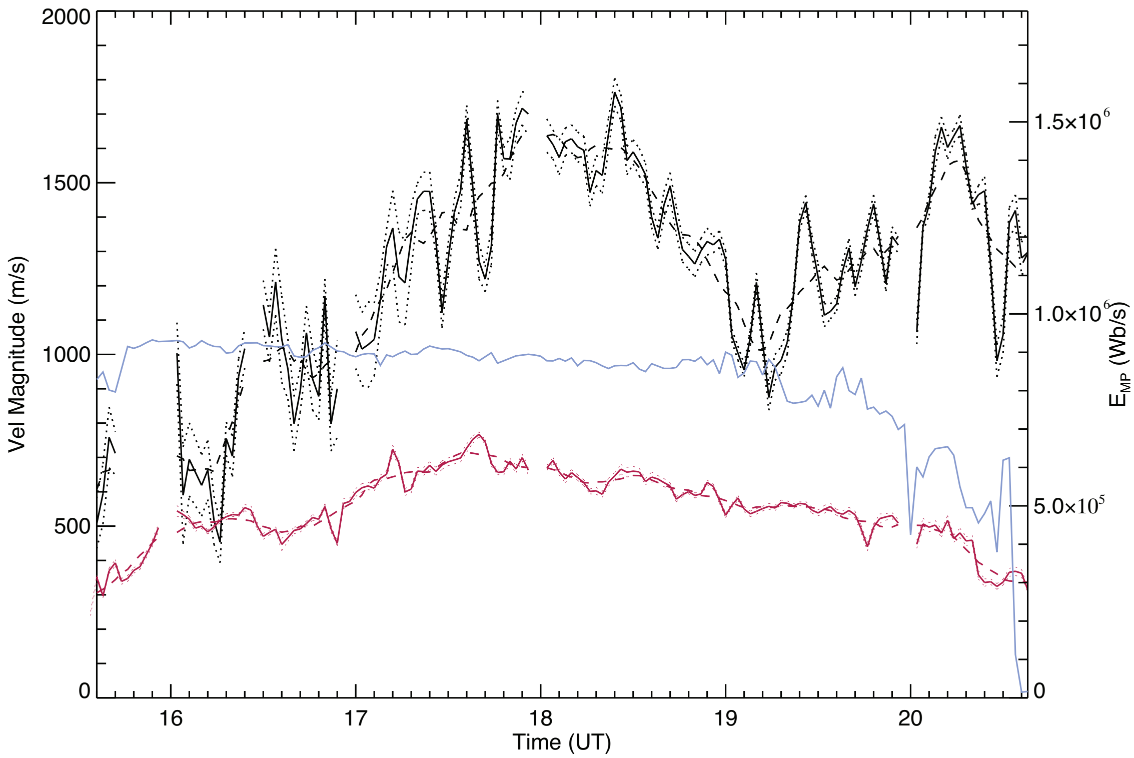

Figure 4. Time series of the solar wind driving function, E_{MP} (blue), the spatially averaged convection in the dayside throat (black) and in the central polar cap (red). The dashed lines are a 16-minute smoothed version of the solid lines.

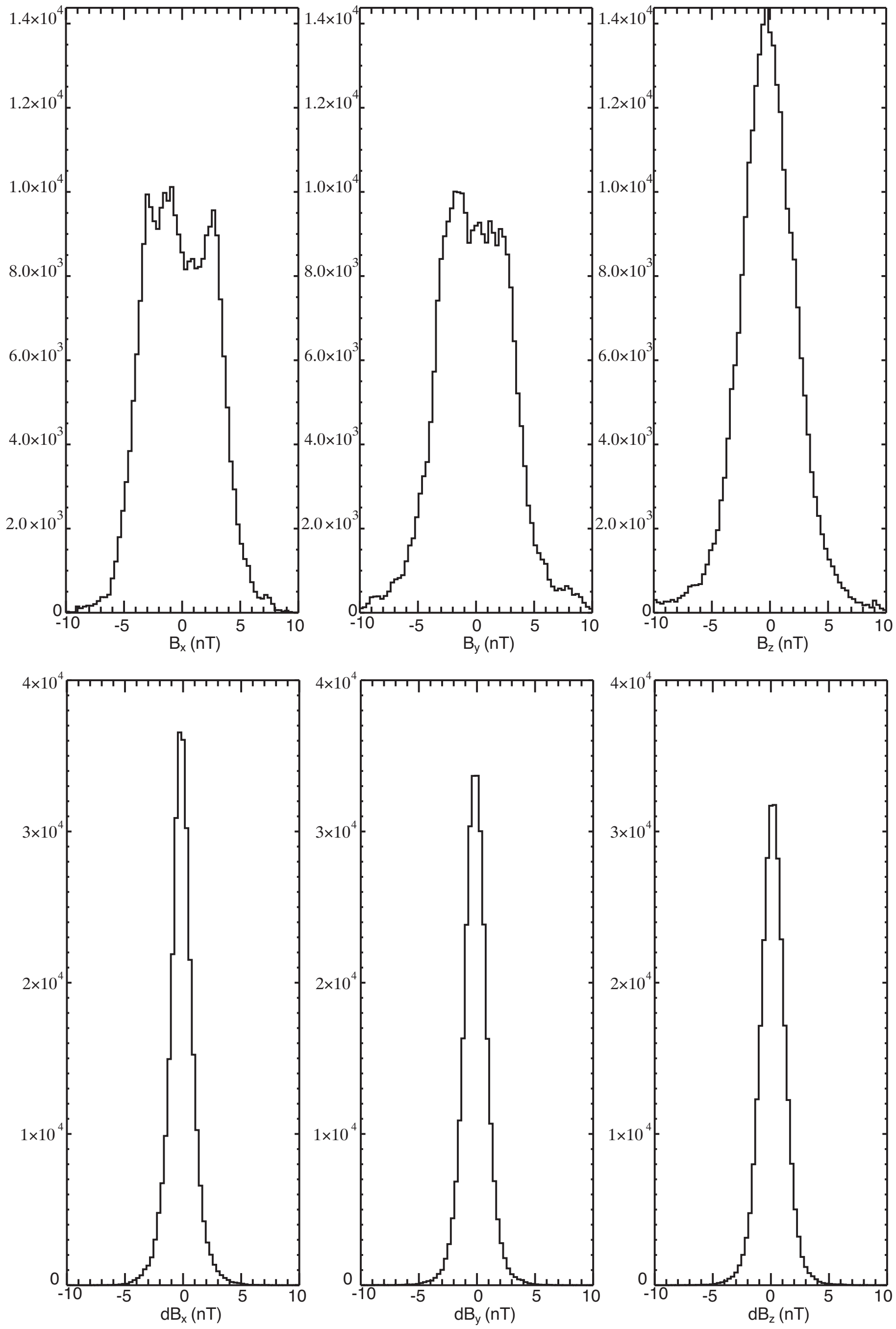

Figure 5. Distributions of the three IMF components, B_x, B_y, and B_z, and their absolute deviations.

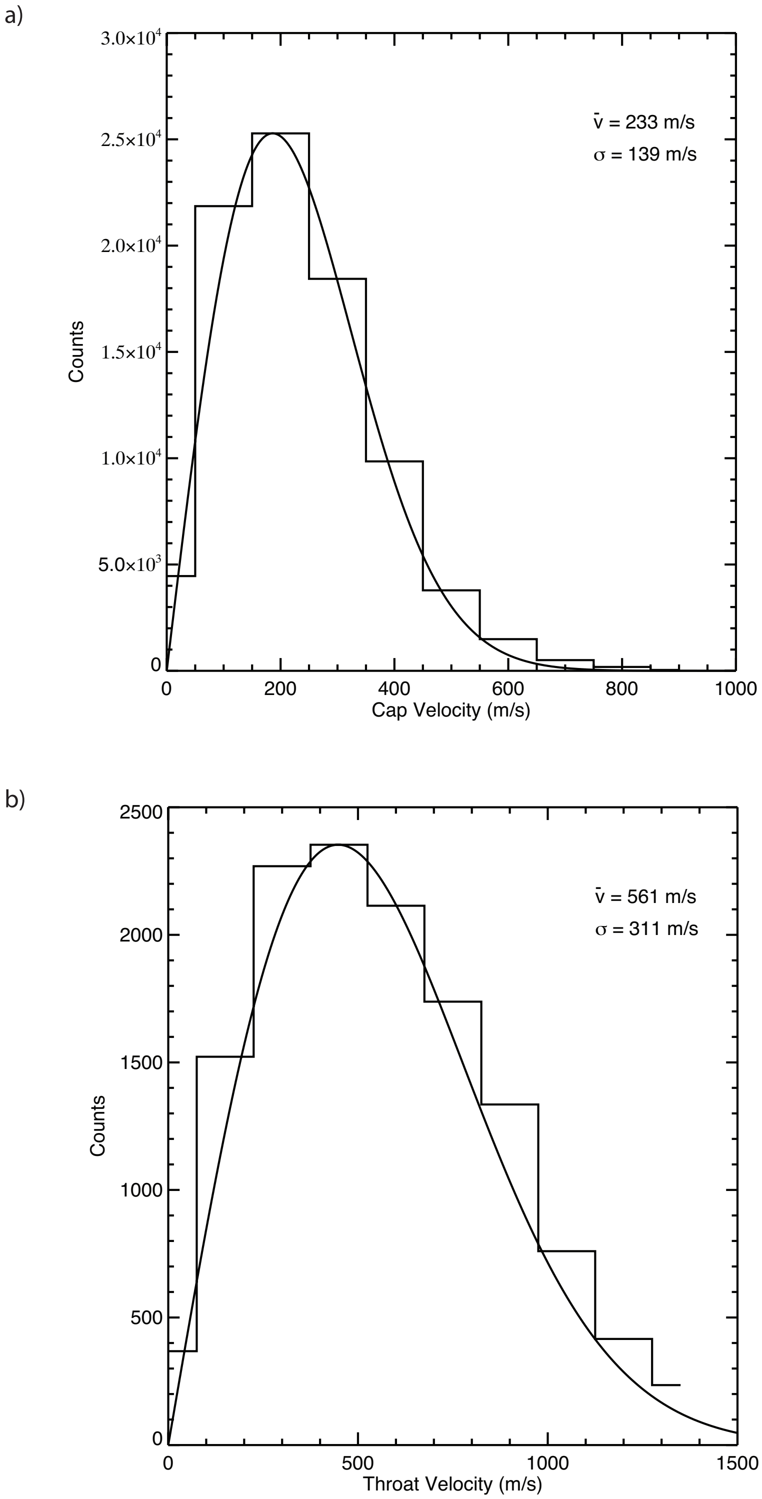

Figure 6. Histograms of observed velocity magnitudes for the total database for (a)the central polar cap, and (b)the region identified as the cusp.

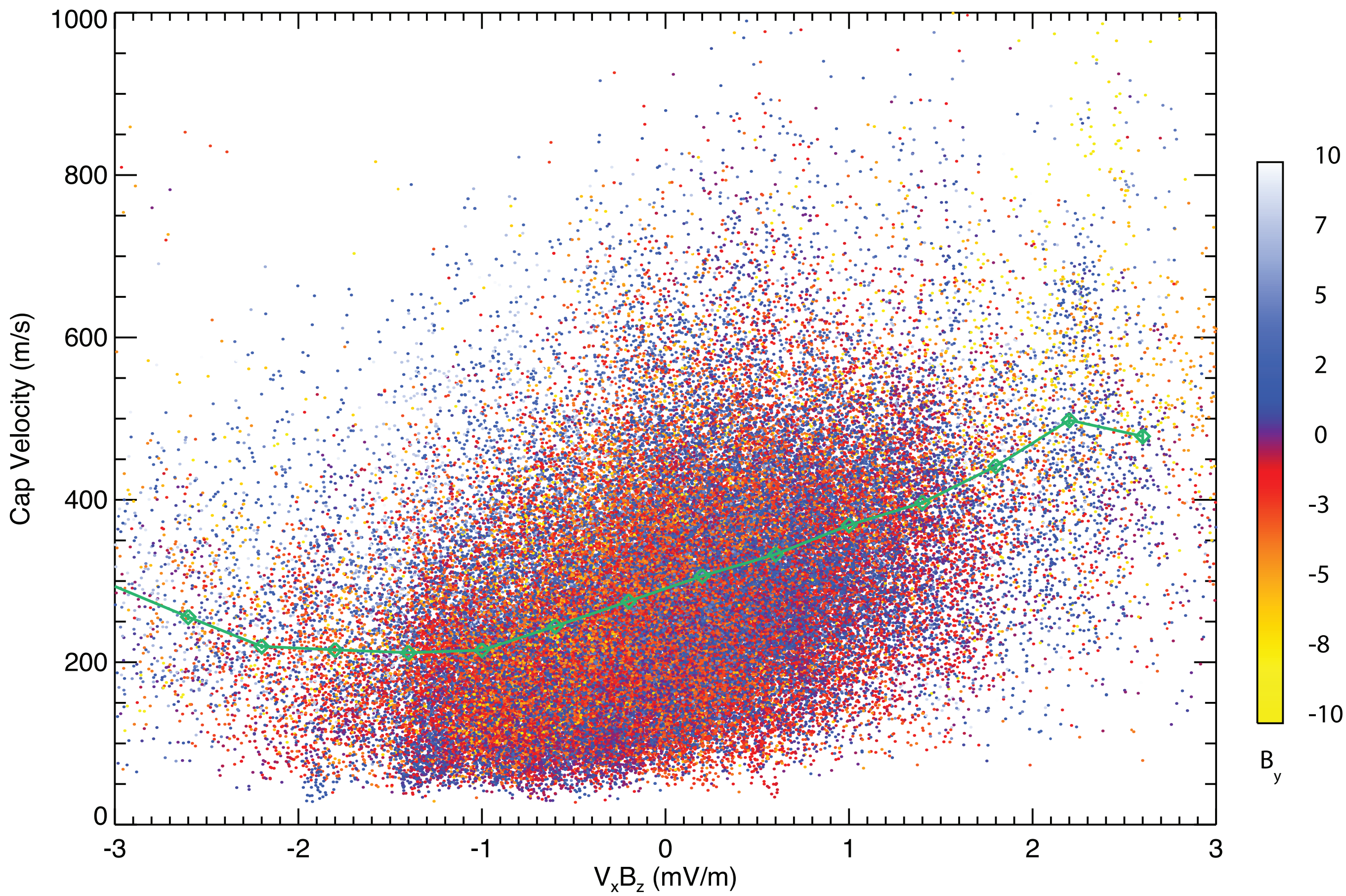

Figure 7. Scatter plot showing the observed velocity in the polar cap versus the product of the radial component of the solar wind velocity with the z-component of the IMF. Each point is an average of all measurements within the 85° latitude circle.

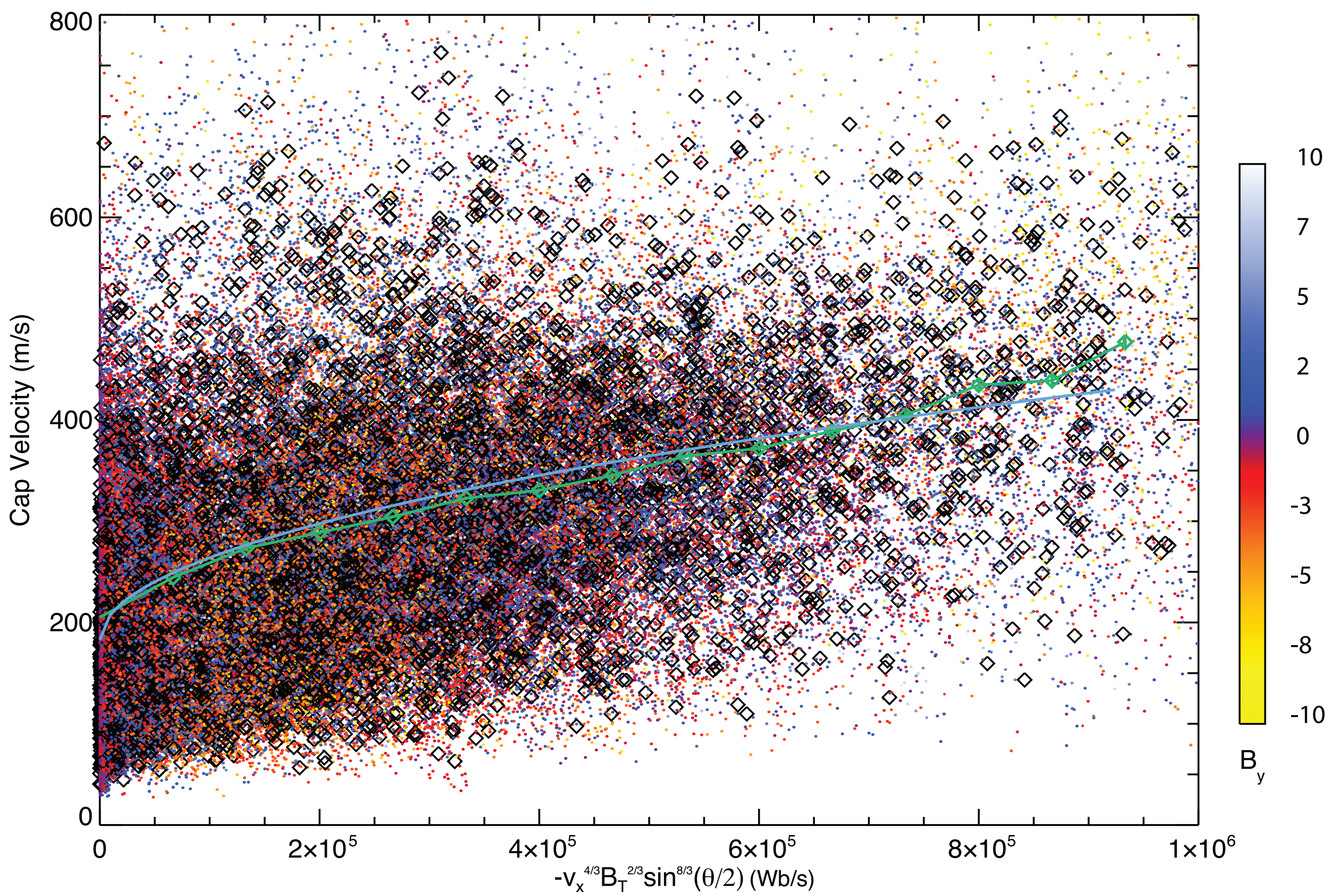

Figure 8. Scatter plot showing the observed velocity in the polar cap versus the E_{MP} parameter. Each point is an average of all measurements within the 85° latitude circle. The black diamonds represent time averages over 15 minutes. The green diamonds and connecting line show the average value in ten bins of E_{MP}. The blue line shows a fit of the averages vs $\sqrt{E_{MP}}$

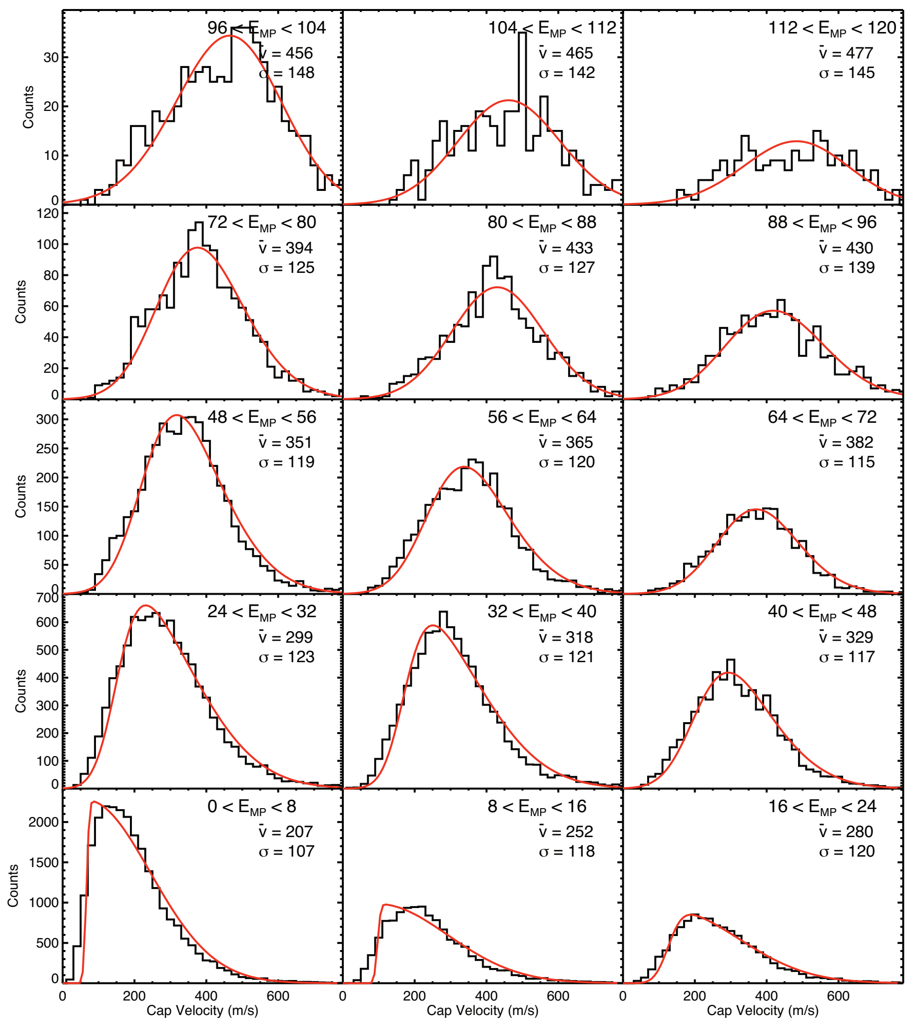

Figure 9. Histograms of observed polar-cap plasma velocity for various levels of the $E_{MP}/10^4$ parameter. The superposed red curves show skew-normal distributions scaled to the peak value of the histograms. The average velocity and standard deviation are given for each E_{MP} level.

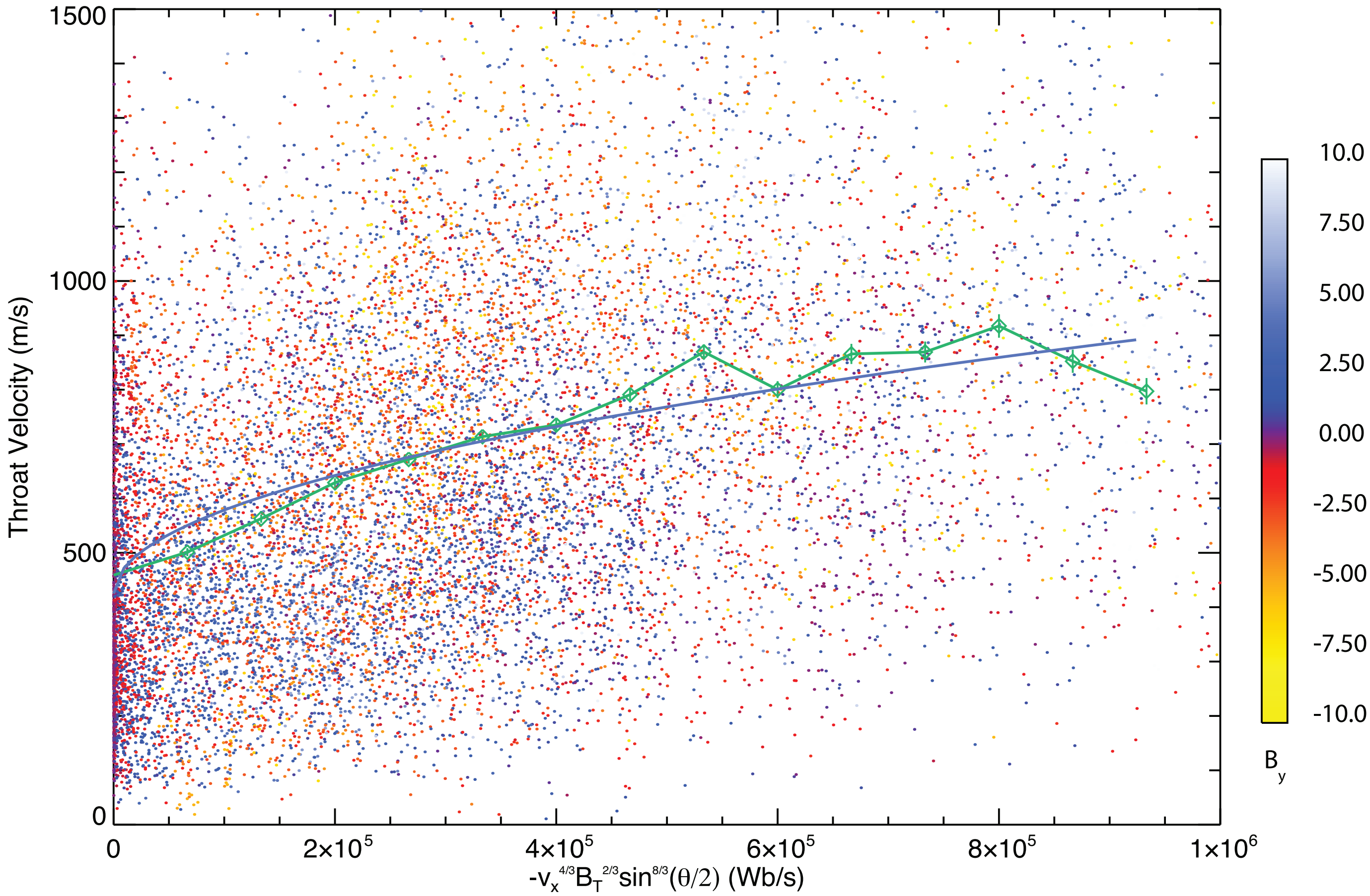

Figure 10. Scatter plot showing the observed velocity in the cusp versus E_{MP}. Each point is an average of all measurements within the 85° latitude circle. The green diamonds and connecting line show the average value in ten bins of E_{MP}. The blue line shows a fit of the averages vs $\sqrt{E_{MP}}$

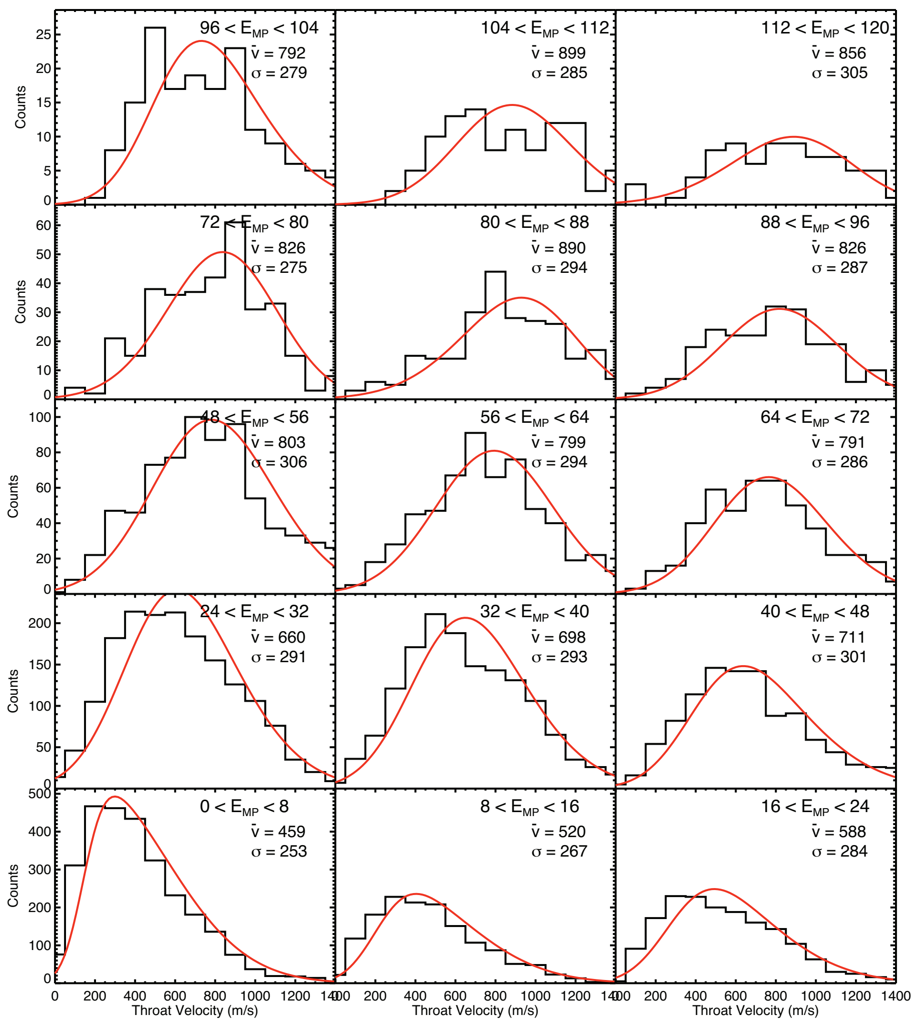

Figure 11. Histograms of observed cusp plasma velocity for various levels of $E_{MP}/10^4$. The superposed red curves show skew-normal distributions scaled to the peak value of the histograms. The average velocity and standard deviation are given for each E_{MP} level.

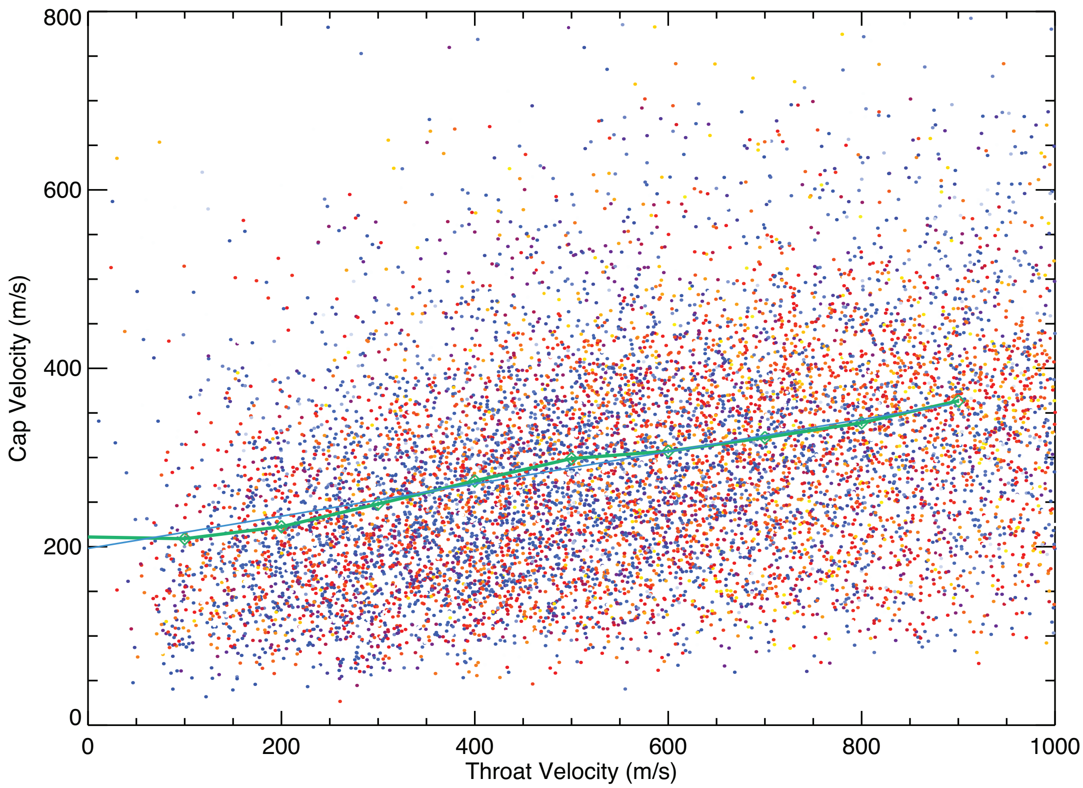

Figure 12. Scatter plot showing the observed velocity in the central cap versus that observed in the dayside throat region. The green diamonds and connecting line show the average value in ten bins of E_{MP}. The blue line shows a linear fit of the averages.